Preventing Glass Alteration in Museum Objects using ALD Deposited Amorphous Alumina Coatings

Miriam E. Hiebert[1,2], Jamie Weaver[3,2§], Thomas Lam[2], Nicole Little[2], Ethan Hyde[1], Edward P. Vicenzi[2,3§], Raymond J. Phaneuf[1,*]

[1]*Department of Materials Science and Engineering, University of Maryland, College Park, Maryland 20742*
[2]*Smithsonian Institution, Museum Conservation Institute, 4210 Silver Hill Road Suitland, Maryland 20746*
[3]*National Institute of Standards and Technology, Materials Measurement Laboratory, 100 Bureau Dr, Gaithersburg, Maryland 20899*

§ Second affiliations are via nonfunded, guest research appointments at listed institutions.
* Corresponding author; phaneuf@umd.edu

Abstract

The chemistry and kinetics of glass alteration have been topics of considerable study and debate over the past several decades. While work is still progressing in understanding the mechanisms by which glass degrades, what has not been as well studied are methods of slowing or preventing the alteration of glass surfaces and objects. This is of significant interest to the heritage science community, where the breakdown of historic glass or glass art objects is proceeding, with few viable options available to museum conservators to mitigate its effects. Experimental measurements using atomic layer deposited (ALD) aluminum oxide coatings on a model silicate glass show a significant reduction of the rate of glass alteration.

Keywords

Glass, glass alteration, atomic layer deposition, ALD, amorphous alumina, glass disease

Introduction

Silicate glass is a thermodynamically metastable phase that over time undergoes chemical and physical alterations to attain a more stable state [1, 2, 3]. Though the process of glass alteration can be slow relative to a human timescale, it presents a complex and pervasive problem in applications where the longevity of the glass structure is important [4, 5]. These applications range from the storage of nuclear waste [6, 7], to maintaining the efficiency of solar cell components [8], to the focus of this work: the preservation of historic glass objects in cultural heritage collections.

Alteration of silica-based glass is a complex process, the kinetics and chemistry of which are dependent on the composition of the glass as well as on the environmental conditions (e.g. pH, temperature, altering solution composition) in which it has aged [4]. The initial alteration of a glass most often takes place via ion-exchange between positively charged water species (H^+ and H_3O^+) and the cationic glass network modifiers (e.g. alkali and alkaline earths) [9]. This is usually accompanied by the hydrolysis of the glass network, which can result in the release of other glass forming species into solution (e.g. Si, Al, and Fe). As alteration proceeds other processes may also occur. For example, a change in solution chemistry may cause the formation of crystalline secondary alteration products, which may in turn change the rate of alteration [7]. Hydrolysis and ion exchange can result in the formation of a hydrated silicate gel layer on the surface of the glass, the swelling/contraction of which produce stress across the interface between the alteration layer and the glass driving crack nucleation [10, 11]. Micro-crack networks in the gel layer and ultimately, the formation of salt precipitates on the surface, may result in a hazed and crusted appearance most often associated with degraded glass as shown in Figure 1 [7]. In museum studies and historical materials conservation literature this phenomenon is often referred to as “glass disease” [5].

Figure 1: Fragments of an altered 18th century French glass wine bottle in the collection of the Smithsonian Institution’s National Museum of Natural History. Excavated by R.K. Harris at Los Adaes in Natchitoches Parish, Louisiana. Photo taken by Anthropology Conservation Lab, Smithsonian Institution.

For the past two decades, one of the most widely accepted models for glass degradation [12] has been based upon the formation of three distinct layers, with a reaction zone (layer 2) forming between underlying bulk glass (layer 3) and a hydrated silicon-oxygen-rich gel altered zone (layer 1) on the surface, illustrated schematically in Figure 2. Following this process, it is often hypothesized that glass alteration is a diffusion-limited process in which the rate of degradation is determined by the interdiffusion of ambient protons into, and cations out of, the bulk glass to form a gel (alteration) layer and a reaction zone [7]. However, recent work conducted by Hellman, et al. [13] suggests that the kinetics of glass degradation could also be reaction-limited, involving coupled glass dissolution and selective re-precipitation of the secondary, hydrated silicate gel layer.

Regardless of which kinetic mechanism limits glass alteration rates, the enabling factor is water or other H-bearing molecular species coming into contact with the glass surface.

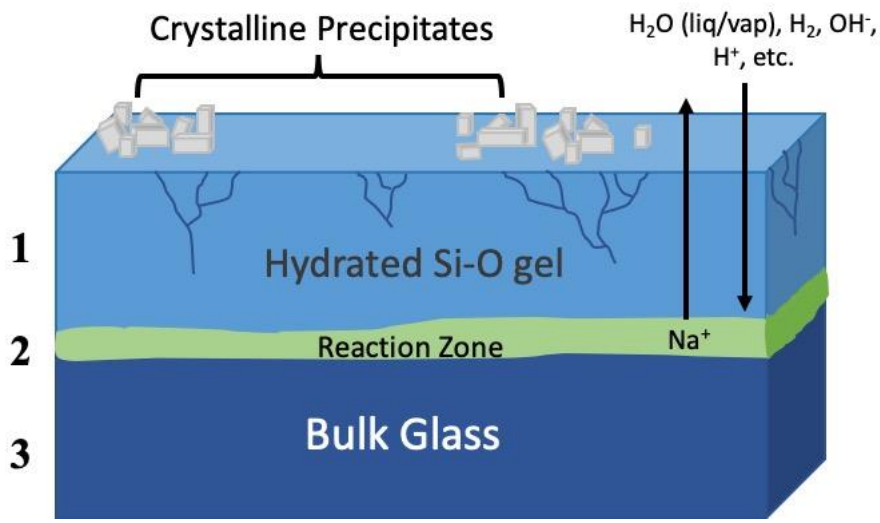

Figure 2: Schematic illustration depicting the three distinct layers of an altered glass surface, assuming a diffusion limited process (adapted from [7])

Therefore, the most effective way to slow glass alteration is to isolate the underlying glass from the ambient reservoir of such species. Currently, very few options exist to markedly slow or prevent glass alteration from occurring. These options include the application of sol-gel silica coatings, which ultimately suffer from the same hydration driven swelling as the glass [14], the application of graphene, which has shown to be effective but is not feasible for application over

large areas [15], and the use of dry cases filled with nitrogen gas in museums, which is effective but expensive to purchase and maintain; this last approach is limited to relatively small, high value objects [16]. The current paper examines the use of atomic layer deposited (ALD) amorphous metal oxide coatings as diffusion barriers for reducing the rate at which water or other H-bearing molecular species come into contact with the surface of glass objects, thereby slowing alteration of these surfaces.

The scope of this paper is on the efficacy of ALD coatings for the mitigation of glass alteration. However, in addition to efficacy, there are other factors that are important to understand prior to the use of new methods as conservation treatments in museums which will not be discussed here. These factors include the effect of the applied coatings on the appearance of the object, and the reversibility of the treatment. Ongoing work to characterize degree of the apparent color change imparted by the applied coatings as well as the relative rates of etching for Al_2O_3 ALD from these glass surfaces will be reported elsewhere.

Methods/Experimental

Glass Samples:

Soda lime float glass, the glass type most typically used in modern windows, is silica based with Na_2O as the primary flux and $Ca(OH)_2$ as a stabilizer. Samples of this type of glass (from a window from a commercial manufacturer (Guardian Glass)) were chosen for this study. The glass has a composition with mass fractions of approximately 0.75 kg/kg SiO_2 and 0.10 kg/kg Na_2O. Other major, minor and trace additives listed in Table 1.

Imaging and Microanalysis:

Light Microscopy

Light optical microscopy images were collected using a HiROX KH-8700 3D digital microscope with an embedded proprietary operating system and software package. Visible light microscopy was used to obtain reflected bright-field montages, each covering an area ≈ 1 cm × 1 cm of the sample surfaces. These images were then processed using a manual thresholding feature in the ImageJ open source software package [17] to binarize the image and estimate the percent area that remained coated with ALD Al_2O_3 or TiO_2 after a period of accelerated aging. This process was performed for images obtained from both of the large faces of each glass sample (approximately 1 cm by 1 cm) yielding an estimate of the percentage of the surface left bare after aging.

Scanning Electron Microscopy and Microanalysis

Electron microscopy images of glass surfaces and X-ray microanalyses to determine the composition of the glass were obtained using a Hitachi S3700N scanning electron microscope (SEM) equipped and a Bruker X-Flash 6|60 energy dispersive spectrometer (EDS). A beam energy of 7 keV and a constant probe current of 2.00 nA ± 0.02 nA was used for these measurements. For calibrandt-based quantified samples, both the calibrandts and samples were carbon coated with a layer thickness ≈ 25 nm using a Cressington 108 Auto/SE sputter coater. A well characterized calibrandt-based quantification method using a Phi-Rho-Z matrix correction routine [18] implemented in the Bruker Esprit V2.2 software package was used to determine glass compositions (see SI Table 1 for a listing of primary standards). Corning reference glasses A and B were used as secondary calibrandts (samples of known composition which are measured prior to the analysis of an unknown sample in order to verify that the compositional

measurements and calculations being used produce accurate results) and the percent deviations from the expected values were found to be less than 7 % for the oxides of all major elements (SI Table 2; [19]).

To mitigate potential effects of glass inhomogeneity, multiple samples taken from random locations on a large glass pane were used in each experiment and the results were averaged. Modern float glass manufacturing processes involve exposure to liquid tin on one side of the window which allows a trace amount of tin to diffuse into that face of the glass [20]. To account for this, the composition was measured on both faces of the glass window.

Table 1: Quantitative EDS compositional data for an uncoated window glass. The mean of 15 measurements from both sides of the float glass is expressed as oxide mass fraction (kg/kg) multiplied by 10^2 for readability. Up is the liquid tin-exposed side and 'down' is the unexposed side. Uncertainty is reported to one standard deviation of the population statistics (n=15, where n is the sample size, per side).

Oxide	Glass (kg/kg x 10^2)	Glass (kg/kg x 10^2)
Face:	up	down
SiO_2	73.56 ± 0.90	75.60 ± 0.76
TiO_2	0.03 ± 0.077	0.08 ± 0.06
Al_2O	0.81 ± 0.10	0.791 ± 0.026
Fe_2O_3	0.11 ± 0.05	0.07 ± 0.03
MgO	3.88 ± 0.14	3.825 ± 0.09
CaO	8.12 ± 0.28	8.11 ± 0.12
Na_2O	12.19 ± 0.57	12.12 ± 0.29
K_2O	0.33 ± 0.02	0.35 ± 0.03
SO_3	0.08± 0.03	0.12 ± 0.02
SnO_2	0.84 ± 0.53	n/a
Total	99.76 ± 1.51	101.06 ± 0.38

ALD Coating:

ALD coatings were deposited on the glass samples using a commercial (Beneq TFS 500) ALD reactor located in the Nano Fabrication Lab at the University of Maryland. This study focused primarily on Al_2O_3 ALD coatings, which have a uniform, near unity transmission across

the visible light spectrum. Therefore, thin alumina coatings (optical path length 2nd << visible light wavelength λ) are not easily detected by human vision and are appropriate for museum applications [21]; for thicker films, optical interference between reflections at the surface and interface with the substrate can lead to visible color shifts [22]. In spite of a nonuniform optical absorption across the visible spectrum, TiO_2 ALD coatings, which cause the glass to appear blue, were also examined in this work owing to a previous report of the relative lack of durability of alumina ALD films in water [23]. The Al_2O_3 ALD coating process used trimethylaluminum (TMA) and water as precursor gasses while TiO_2 ALD used tetrakis(dimethylamido)titanium (TDMAT) and water as precursors. Figure 3 depicts a schematic of the idealized deposition process for Al_2O_3 ALD.

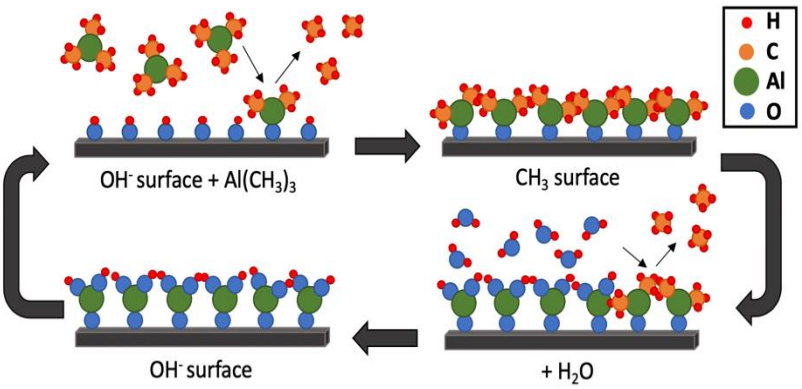

Figure 3: Schematic of the chemical steps in the idealized depostion of Al_2O_3 ALD.

Exposure and purge times for the precursor gases were determined empirically based on perceived color uniformity across a Si wafer that was included in the reactor chamber during each deposition experiment; gradients in the local pressure within the reactor lead to thickness variations if the individual reactions do not reach saturation The pulse/purge times suggested by the ALD reactor manufacturer were found to be insufficient for coating the silicon wafers, and presumably the silicate glass samples uniformly. Therefore, the suggested precursor exposure and purge times were quadrupled, resulting in a uniform visual appearance; these resulting times are listed in Table 2. All depositions discussed here were performed at 150 °C.

Table 2: Precursor exposure and purge times used for the deposition of Al_2O_3 and TiO_2 ALD films onto commercial float glass.

ALD Deposition Parameter		
Metal Precursor Chemical	Al_2O_3 trimethylaluminum (TMA)	TiO_2 tetrakis(dimethylamido)titanium (TDMAT)
Exposure time (s)	2	1
$Purge_1$ time (s)	2	0.5
H_2O exposure time (s)	2	1
$Purge_2$ time (s)	2	0.5

A custom support was developed for coating these samples, consisting of 1 mm diameter glass spheres (Sigma Aldrich) that were low-temperature-fused to a thin glass sheet. This allowed for the elevation of the samples, aiding exposure of the bottom surfaces of the substrate to the ALD precursor gases. Samples were flipped over halfway through each coating process to expose the contact points that the sample made with the support and to promote complete sample coating.

Coating Thickness

Subsequent to sample coating, the average thickness of the applied ALD coatings versus the number of deposition cycles was determined by spectroscopic ellipsometry. The ellipsometry was performed on a Woollam M2000 spectroscopic ellipsometer. Both a tungsten filament and a deuterium bulb light source were used to cover a wavelength range of 190 nm –1800 nm. These analyses were performed with the instrument in horizontal mode due to the weight of the samples. The proprietary Woollam software package CompleteEase was used to build sample models, including optical constants and film and substrate parameterization, and to fit the resulting data. Results are reported in Table 3.

The Al or Ti signals obtained via SEM-based μXRF were measured for increasing numbers of cycles of ALD deposition. The relationship between the μXRF output and

ellipsometry thicknesses was found to be highly linearly correlated as the number of ALD deposition cycles is increased beyond an initial transient (discussed below). Taking advantage of this correlation, the μXRF signal was used to estimate the ALD coating thicknesses. The μXRF analysis was performed under high vacuum in the SEM using a Bruker XTrace μXRF with a 50 kV polychromatic Rh source and an X-ray optic that produced a 33 μm (measured at Cu Kα) elliptical spot with an approximate area between 900 μm^2 and 1000 μm^2. X-ray spectra were collected for 60 live seconds. Using Bruker Esprit v2.1, the resulting X-ray scatter was background fit using a spline interpolation of non-peak channels and peaks were fitted using Gaussians with overlapping X-ray lines deconvolved to yield the net counts of Al or Ti that represent the sum signal resulting from the glass substrate plus the ALD thin film [24]. The results for both ellipsometry and μXRF analysis are reported in Table 3.

Surface Topography

The surface topography of the ALD coated and uncoated samples was characterized using a Digital Instruments Dimension 3100 atomic force microscope (AFM) in tapping mode with a 300 kHz resonant frequency silicon cantilever (Nanosensors) with a nominal 10 nm terminal tip radius; maps were recorded for the silicate glass samples as a function of the number of ALD deposition cycles. Glass samples were cleaned using sonication in a series of stock grade solvents (isopropanol, acetone, methanol, deionizied (DI) water) prior to analysis. The RMS (root-mean-square average of the deviations in profile height from the mean) roughness was determined, based on scans of 5 μm x 5 μm lateral dimensions across these surfaces, using the Bruker NanoScope (R) IIIa software package, version 5.33R1sr1.

Accelerated Aging:

As glass alteration under ambient conditions is a slow process on laboratory time scales even in the absence of barrier coatings, a method of artificial accelerated aging, involving immersion of glass in water at an elevated temperature, was employed. An ASTM standard method was adapted for evaluating product stability of industrially produced windows (ASTM-PCT C1285) [25]. The original method calls for using a monolith of glass and sealing it in a polyflouroalkoxy polytetrafluoroethylene (PFA PTFE)-fluorocarbon vessel with a known amount of ultrapure water at elevated temperature for a given amount of time. In this study small blocks of glass, each with mass of 1.00 g ± 0.05 g (as determined by weighing each sample and selecting only those with weights measured within this range), and dimensions of ≈ 0.5 cm in thickness, and ≈ 1.0 cm by 1.0 cm in length and width were cut. Glass samples were cleaned using sonication in a series of stock grade solvents (isopropanol, acetone, methanol, DI water), and then placed in individual TFE vessels (Savillex) along with 10.00 mL ± 0.04 mL of ultra-high purity DI water, with an initial measured resistivity of approximately 18 MΩ-cm (Millipore Milli-Q Integral 3 water purification system). The vessels were then placed in an oven (Quincy Lab Inc., 10GC Gravity Convection Oven) held at 90 °C ± 5 °C, for prescribed lengths of time. At the end of each accelerated aging experiment the glass was removed from its vial, allowed to dry in atmosphere, and then stored for subsequent analysis. Samples of glass, coated via ALD with a range of thicknesses of either Al_2O_3 or TiO_2 oxides, were subjected to the same method of accelerated aging described above for aging uncoated glass. To account for variation in the samples and the aging method, generally multiples of six samples were aged simultaneously (an exception was for an aging experiment of 336 h ± 4 h (≈ 14 days) of aging uncoated glass, where the number of samples was 12) in each experiment; the results for the multiple samples were

averaged. For uncoated glass samples the immersion time was varied from (24 to 336) h ± 4 h. For the majority of the aging experiments on ALD coated samples an immersion time of 336 h ± 4 h was used; an exception to this was one experiment where glass coated with 1000 cycles of Al_2O_3 ALD was aged for 168 h ± 4 h (≈ 7 days).

ICP-MS Analyses:

Subsequent to aging, the aqueous solution from which a sample had been removed was analyzed for the concentration of Si and Na leached from the glass. This was done using a GBC Optimass 9500 Time-of-Flight Inductively Coupled Plasma-Mass Spectrometer (ICP-MS). For this analysis, 0.1 g aliquots of the sample water were diluted to a total weight of 50.0 g using 18 MΩ-cm ultrapure water. An internal standard (High-Purity Standards IS-2) was added to each sample in 0.2 g aliquots and was used to track the stability of the instrument and the accuracy of the analyses over time. Calibration of the instrument was done using two different multi-element standard solutions containing the elements of interest (High-Purity Standards 68 Component ICP-MS Standards A and B). The dilutions, concentrations, and contents of all three standards used can be found in SI Table 3. Analyses were run in sets of ten for each sample measured and the relative standard deviations output by the instrument software (Optimass version 2.2) were found to be on average 4.2 % for Na and 4.1 % for Si.

In addition to analyzing the aqueous leachate, analyses were also performed on three samples of water that had not been in contact with a glass sample but that had been subjected to identical aging and storage conditions to serve as aqueous “blanks”. The values measured from these blank samples were averaged and the average concentrations were subtracted from the values obtained from the leachate that had contained the glass samples. The resulting

"background" corrected concentrations, determined for each of the multiple samples with a given coating type, coating thickness, and aging time were averaged together and the resulting mean values are reported in Figure 6 to one standard deviation of the population statistics.

Results and Discussion

Characterizing ALD Coatings on Glass:

While ALD on chemically uniform surfaces such as Si wafers has been relatively well studied [26, 27], deposition on chemically inhomogeneous surfaces is less well understood [28, 29]. Characterization of the uniformity, or "conformality" of the applied coatings to the substrate was needed to determine the number of ALD cycles needed to cover the surface of the glass completely, and to investigate possible defects in the applied film.

Coating Thickness

Initial characterization of the ALD coatings included assessing the thickness of the applied coatings on the glass surfaces. Table 3 and Figure 4 summarize the coating thicknesses as measured by ellipsometry and the corresponding μXRF measurement output for each ALD coating and thickness studied.

Table 3: Table listing the results of thickness values determined by ellipsometry (on both the uncoated glass sample (n = 3) and included Si wafer (n = 1)) and the elemental signal obtained from the coated samples via µXRF (n = 5). Growth per cycle (GPC) is reported based upon these results. Uncertainties are reported as the square root of the measured value for the ellipsometric measurements on the Si wafer and as one standard deviations of the population statistics obtained for all other measurements reported.

Cycles ALD	**Al_2O_3 ALD** *GPC ≈ 0.17 nm/cycle, ≈ 74 counts/cycle*			**TiO_2 ALD** *GPC ≈ 0.06 nm/cycle, ≈ 52 counts/cycle*		
	Thickness from Ellipsometry (nm)		µXRF Al K_α (net counts)	Thickness from Ellipsometry (nm)		µXRF Ti K_α (net counts)
	Glass	Si wafer	*n=10*	Glass	Si wafer	*n=10*
0	0	0	1833 ± *543*	0	0	1444 ± *38*
25	0.7 ± *0.8*	4.1 ± 2.0	3508 ± *467*	n/a	n/a	n/a
50	2.3 ± *1.5*	8.1 ± 2.8	4803 ± *645*	n/a	n/a	n/a
100	17.9 ± *7.9*	15.8 ± 4.0	8840 ± *843*	5.3 ± *0.3*	6.1 ± *2.5*	4861 ± *69*
200	32.5 ± *4.2*	31.0 ± *5.5*	14861 ± *1932*	14.1 ± *0.0*	12.4 ± *3.5*	11681 ± *108*
500	90.1 ± *2.1*	99.3 ± *9.9*	34949 ± *3078*	39.8 ± *5.5*	33.1 ± *5.7*	30279 ± *174*
1000	172.2 ± *2.1*	185.1 ± *13.6*	74278 ± *4643*	59.0 ± *7.7*	57.1± *7.5*	52366 ± *228*

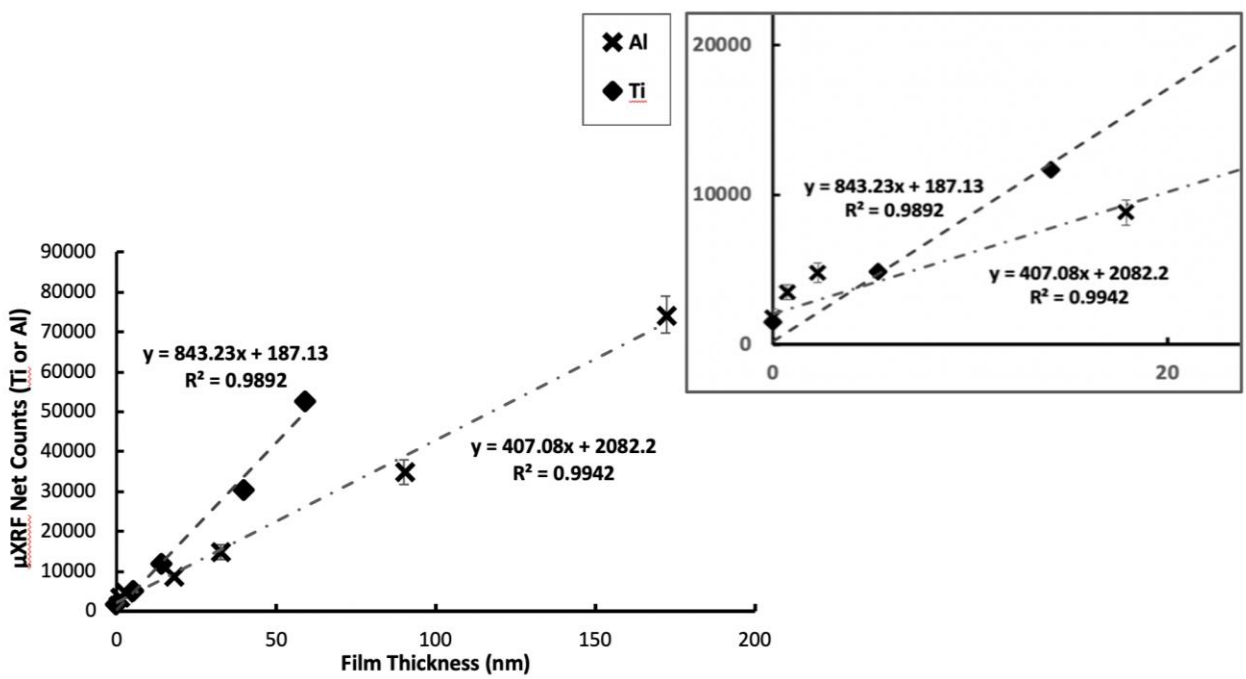

Figure 4: Graph showing relationships between coating thickness values, determined with ellipsometry, and µXRF signals. It should be noted that the base glass itself contains small concentrations of both Al (1833 net counts) and Ti (1444 net counts), resulting in measured signals from both elements measured on the uncoated glass and accounting for the non-zero y-axis intercepts of the linear regression fits, shown as dashed lines. Error bars represent one standard deviation of the population statistics, however, these values, which are also reported in Table 3, often result in error bars that are too small to be seen in this figure.

A linear relationship between the ellipsometrically measured coating thicknesses and the net counts of Ti and Al measured using μXRF can be seen in Figure 4, with regression cefficients given in the figure. The non-zero y-intercepts obtained from the linear fits of the data shown in this graph are consistent with the pressence of small amounts of both Ti and Al in the base glass composition. The uncertainties in the linear fits were calculated for both ALD coatings. For the Al_2O_3 ALD measurements, the resulting linear fit was found to have a slope of 406 ± 16 net counts/nm, and a y-intercept of 2154 ± 1316 net counts which is indistinguishable from the measured value for net counts of Al in the base glass (1833 ± 543 net counts) within the statistical uncertainty. Similarly for the measurements made on the TiO_2 ALD coatings, the slope was found to be 863 ± 68 net counts/nm and the y-intercept to be -737 ± 2470 net counts, while the measured value of Ti net counts in the base glass was determined to be 1444 ± 38.

The measured value of Al and Ti in the base glass were found to be within one standard deviation of the y-intercepts obtained from the fits for each coating. However, it is interesting to note that there is a systematic deviation apparent between data and the linera regression fits, particularly for Al_2O_3 ALD coatings for small numbers of coating cycles, which can be attributed in a deviation from layer-by-layer growth. It is apparent for these thinner coatings of Al_2O_3 ALD, the initial thickness shows a sublinear dependence on the number of deposition cycles. Following standard practice, during each of these coating experiments, a control Si wafer was placed inside the ALD chamber along with the glass samples to allow for an estimation of the applied coating thickness on an ideal substrate. A large discrepancy between the thicknesses measured on the control wafer and the glass samples was noted for the thinnest Al_2O_3 ALD coatings (Table 3), with the latter values initially being consistently lower. This suggests that the precursors are reacting less readily with the glass surface than with the Si wafer, which may be

due to locally unfavorable surface terminations on the glass. We hypothesize that island nucleation and growth occur in the early stages of the formation of these coatings [26, 28].

Roughness of Sample Surfaces

A test of the hypothesis that ALD coatings nucleate and grow as multilayer islands, rather than homogenously in a layer-by-layer manner, is possible via measurement of the surface topography: if correct, evidence should be observable as a transient increase in the roughness of the surface [30]. While it can be difficult to identify small islands of film on a rough substrate, the AFM height maps indicate a transient increase in the observable surface roughness, consistent with island nucleation and growth leading to some degree of coalescence (Figure 5). In addition to the topographic maps, Figure 5 displays plots of the average RMS roughness measured as a function of coating thickness for both Al_2O_3 and TiO_2 ALD coatings.

The peak value of the RMS surface roughness, measured for an Al_2O_3 ALD dose of 50 cycles (≈ 2.3 nm), was found to be approximately 3 times larger than that of the uncoated glass and on the asymptotic value; this is qualitatively consistent with island nucleation, followed by subsequent lateral, as well as vertical growth [28]. The onset of roughening and island formation seemingly requires higher doses for the TiO_2 ALD coatings, which in turn suggests a lower reactivity of TDMAT, as compared to TMA, with the silicate samples. For both the Al_2O_3 and TiO_2 ALD coatings the intial increase in roughness was followed by a gradual drop with increased coating thickness. This behavior is consistent with growth and at least partial coalescence of multilayer islands at longer deposition times [30].

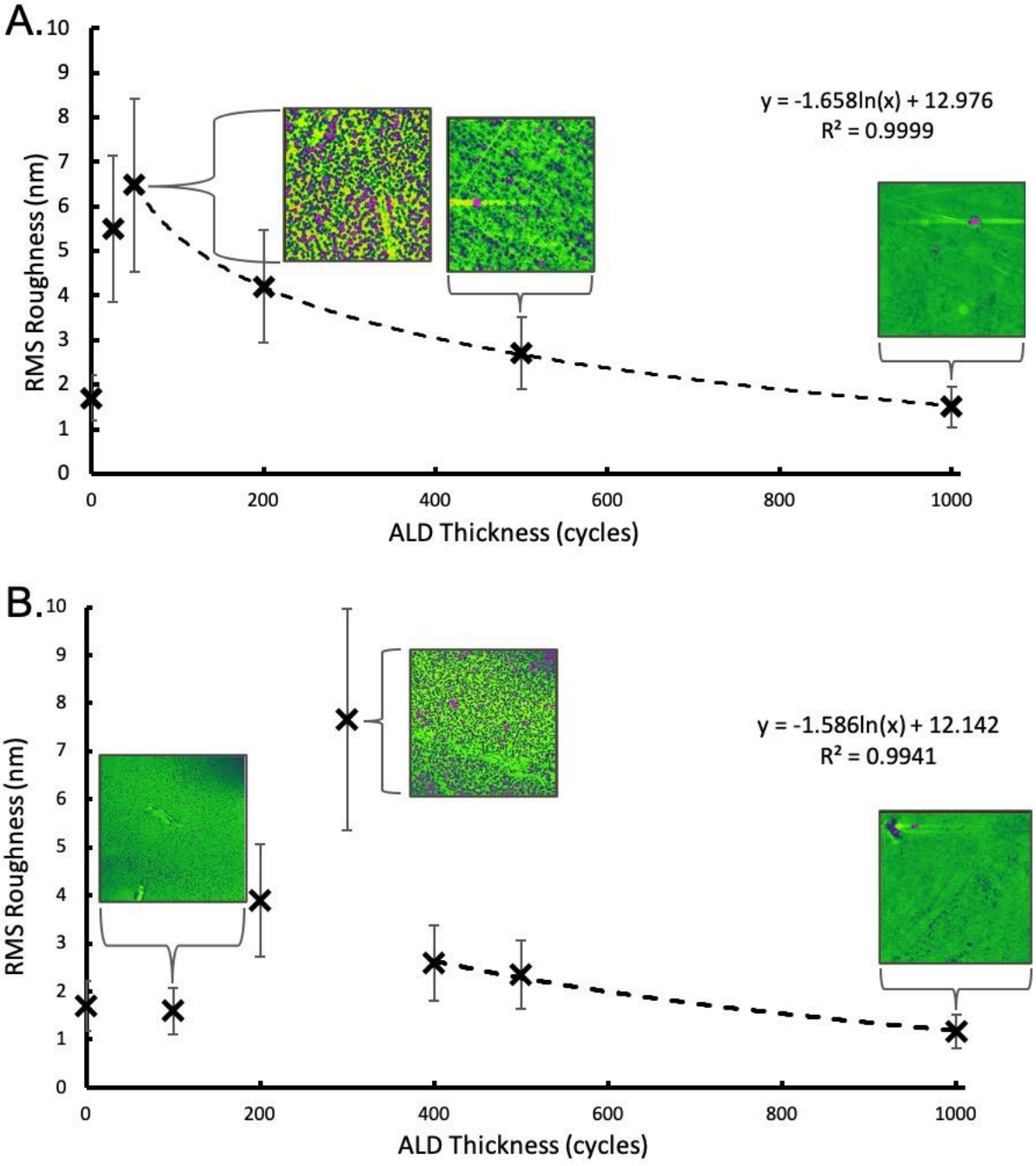

Figure 5: Plots of the average, from multiple measurements across a single surface, RMS roughness measured on samples of float glass with increasing numbers of applied deposition cycles of (A) Al_2O_3 and (B) TiO_2 ALD (in graph B the measurements for doses of 200 cycles, 300 cycles and 400 cycles were obtained at a later time from the rest of the measurements shown). Thumbnail images show AFM topographic maps of selected sample surfaces where the field of view is approximately 10 μm × 10 μm area (green is shallow while purple represents peaks). It has previously been shown that for AFM measurements where the features of interest are at least double the radius of the AFM probe tip, the instrumental uncertainty is estimated to be less than 15 % of the measurement [31]. Uncertainties are reported here to 30% of the measured value for n = 1.

Glass Alteration Studies

Uncoated Glass

It was first necessary to characterize the alteration of float glass without any applied ALD coating under the accelerated alteration method described previously in order to determine the effect of an ALD coating on the glass alteration rates. The graph shown in Figure 6 presents the average measured concentration of Si and Na, that presumably had leached from the uncoated glass, as a function of aging time. The concentrations of these species are used as a metric of glass alteration as their increasing concentration in the leachate should scales with their depletion in the glass matrix [32]. As can be seen from these results, an initial and rapid alteration in the first three days was followed by a plateau in alteration as aging time increases. This is consistent with previously reported glass alteration studies [6, 7].

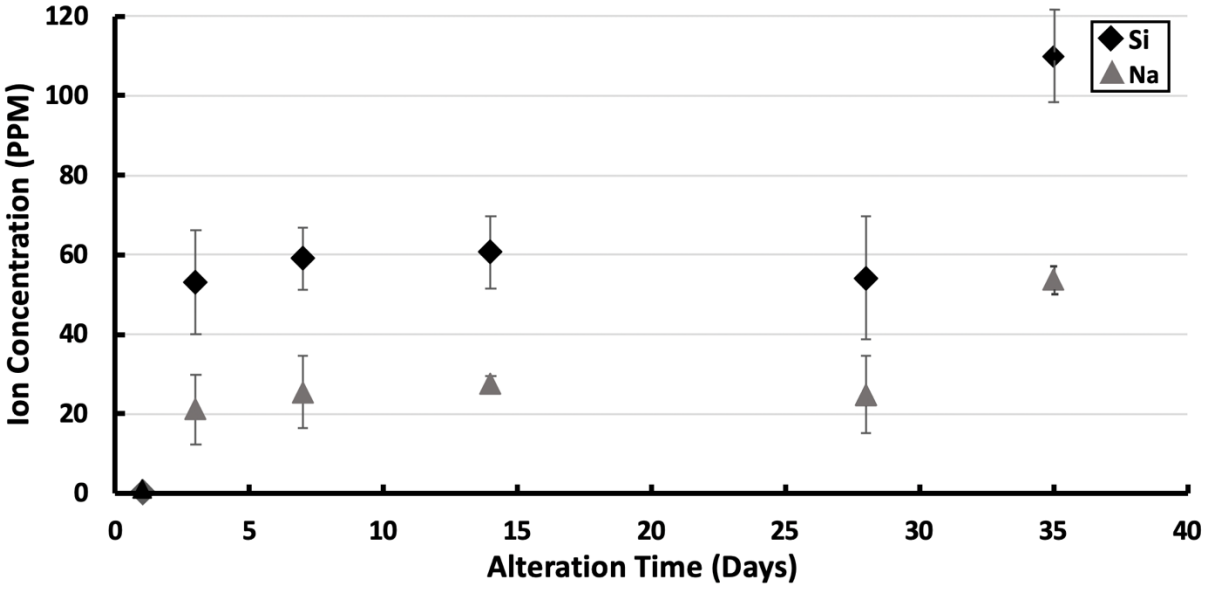

Figure 6: Solution-ICP-MS data showing average concentrations measured for Si and Na present in the water used in accelerated aging of uncoated glass samples after increasing accelerated aging time (n = 6; except for 14 days aging where n = 12). Uncertainties are shown to one standard deviation of the population statistics.

Coated Glass

Solution-ICP-MS analyses were performed on the aqueous solutions used in the accelerated aging tests of the ALD coated glass samples. The average Si and Na concentrations measured after 14 days of accelerated aging in each experiment are shown in Figure 7. While concentrations of Ti were not measured in these samples due to instrumental constraints, Al concentrations were recorded and found to be negligible ($\cong 0$). From the Na and Si data it is observed that Al_2O_3 ALD coatings that result from ≈ 50 growth cycles, corresponding to ≈ 2.3 nm thick films, show a significant drop in the amount of Na and Si lost from the glass. This suggests that thin coatings of amorphous Al_2O_3 films on glass surfaces can profoundly slow the rate of glass alteration.

An alternative interpretation of the decrease observed in this data is that dissolved species are being taken up into newly formed solid phases prior to the leachate measurement. This phenomenon has been reported previously for other silicate-based glasses and may be the result of excess Al in the alteration environment [33]. Such an interpretation however would not obviously be consistent with the supposition that the increasing concentration of Na and Si in the leachate should scale with their depletion in the glass matrix. Additional experiments are underway to allow us to distinguish between these interpretations.

The results obtained from analysis of the water used in aging Al_2O_3 ALD coated samples contrast sharply with the results obtained from analysis of the water used in aging TiO_2 ALD coated samples as shown in Figure 6. No statistically significant decreases were observed in the either the Si or Na concentrations, measured from TiO_2 ALD coated samples (Figure 6A), as

coating thickness was increased.

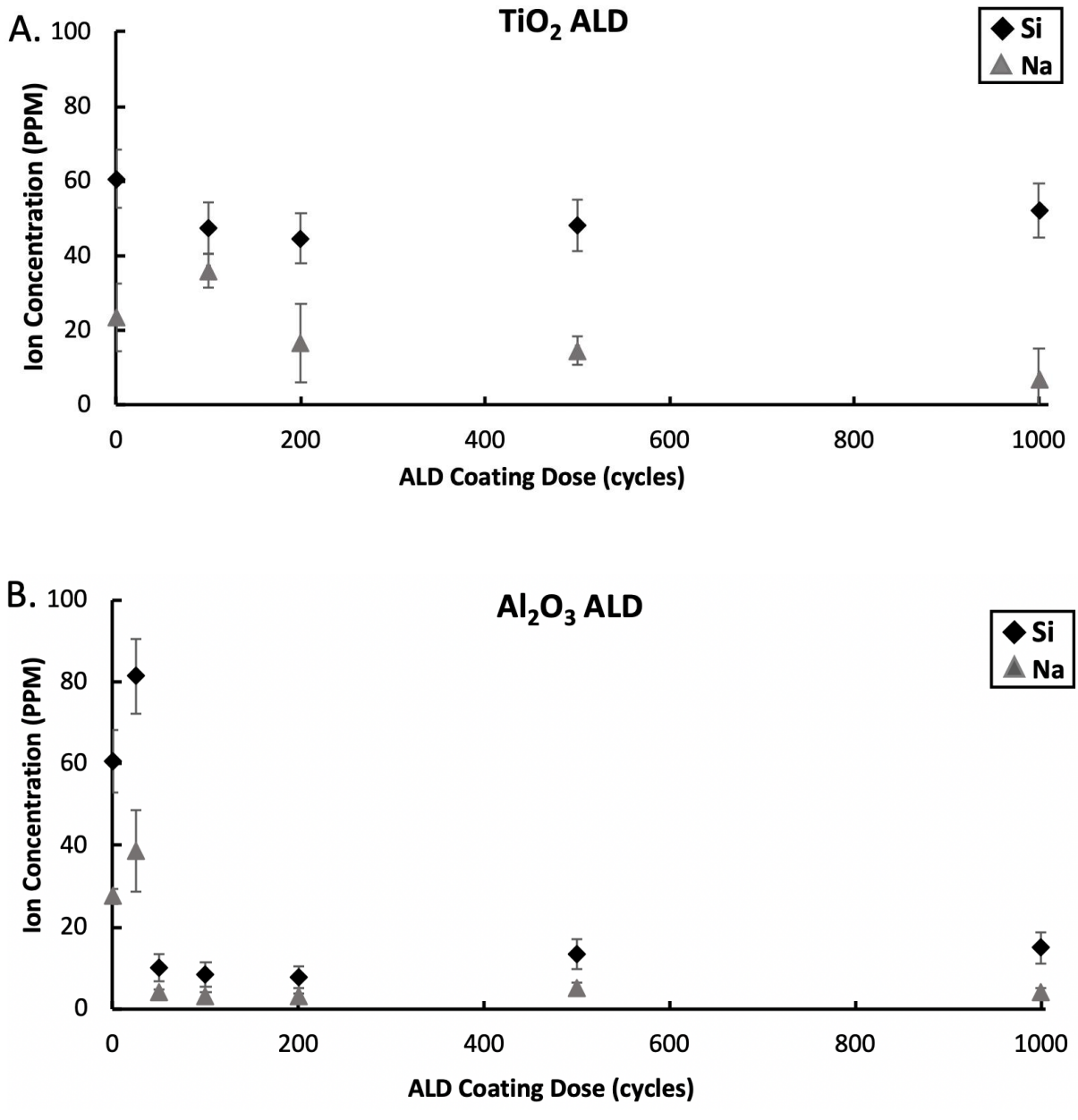

Figure 7: Si and Na ion concentration data obtained from the water from the 14 days +/- 4 hours of accelerated aging of samples of float glass that had been coated with increasing numbers of deposition cycles of (A) TiO_2 ALD and (B) Al_2O_3 ALD. Points plotted at zero cycles show data obtained from glass samples without any applied coatings (also shown in Figure 6). Multiple samples were aged (n = 6) for each coating and relative thickness reported. Uncertainties reported to one standard devation of the population statistics.

The ICP-MS data indicates that while there is a significant decrease in Si and Na loss for Al_2O_3 ALD coated glass samples (Figure 6B), the loss values remain measurable even for the

thickest films investigated. However, even defect-free films allow interdiffusion of Na and Si under ambient conditions giving rise to finite loss but this should fall off with a characteristic thickness dependence not observed here [34]. Indeed, the bulk of the loss of Na and Si measured for the thickest films is likely attributable to the presence of uncoated areas on the glass as shown in Figure 8 and is discussed in the next section.

ALD Coatings After Aging:

Appearance

After accelerated aging for 14 days, the coated glass samples were removed from the aqueous solutions and visually inspected. It was immediately apparent that significant coating loss had occurred during immersion in hot water. The surface of the samples appeared rough and pitted, and with greater scrutiny using various microscopic methods (see Figure 8), it was apparent that large areas of localized coating were lost during alteration. We postulate that these bare areas may result from the expansion of smaller defects in the ALD films (discussed below), which allow local alteration of the underlying glass; if so, expansion of the altered regions due to hydration could cause the coating on the surrounding surface to flake off. Such bare areas were observed to various degrees on all samples after accelerated aging treatment. Similar behavior has been observed previously in other thin film coatings exposed to ambient humidity [35, 36].

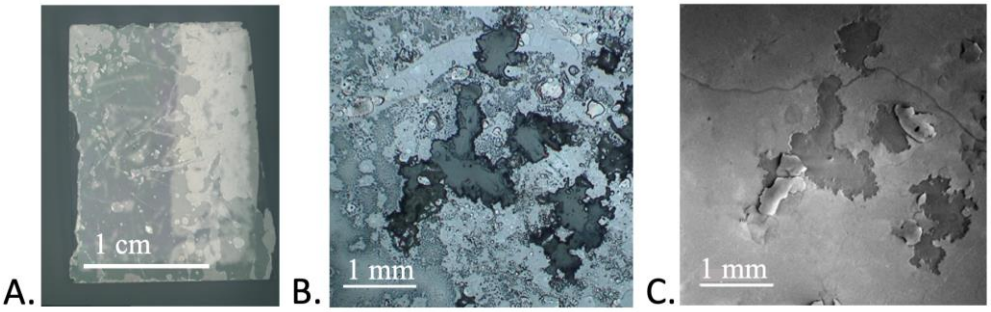

Figure 8: Post-accelerated aging (14 days) micrographs of ALD coated glass. (A) Tiled reflected bright-field micrographs of a sample surface that has been coated with 90 nm Al_2O_3 ALD, (B) reflected bright-field micrograph of a region showing delamination and the glass substrate on sample that had been coated with 26 nm of TiO_2 ALD, and (C) a secondary electron image of the same delaminated region in (B).

Estimating the Fraction of Exposed Glass Surface

To attempt an understanding of the formation and effect of bare areas on the performance of the ALD films as water permeation barriers it is necessary to begin with a rough assessment of the approximate fraction of the uncoated surface area following aging. An example of an original image and the processed binary image of a sample on which partial delamination of a film during aging has occurred can be seen in Figure 9. The contrast of the thin film and base glass in this case exist in reflected bright field because the optical properties of the film and glass are different in reflectance.

Figure 9: A. Tiled-visible light micrograph-image of a surface of a float glass sample that had been coated with 90 nm of Al_2O_3 ALD and subsequently exposed to 14 days of accelerated aging and B. the same image after contrast thresholding. The binary image, B, is comprised of white pixels representing remaining ALD coating, and black pixels that represent exposed glass substrate.

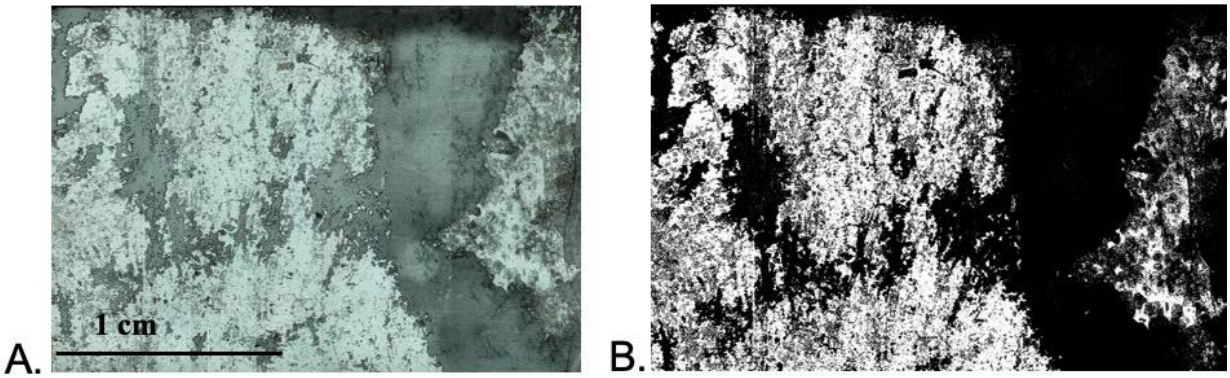

The results of these measurements for several of the ALD coatings examined are presented in Table 5. The measured spatial resolution for this optical microscope and these samples was found to be ≈ 2 μm. As a result, closely spaced (≤ 2 μm) fissures and pinholes were not detectable by this imaging method. Therefore, the values given in Table 4 represent an upper limit on the fraction of the surface still coated. Additionally, this resolution constraint also prevents the detection of any closely spaced defects or pinholes that are present on the surface of the ALD coating prior to aging.

Table 4: Average percentage of coating remaining on the surface of samples of glass coated with a given number of cycles of Al_2O_3 ALD and subjected to accelerated aging at a given temperature for a given length of time. The accelerated aging experiments were run over 14 days unless otherwise indicated. One experiment was run for half that time, as indicated below. Uncertainties were calculated to one standard deviation of the population statistics measured from all samples of each coating type with n = 6.

ALD Method	Cycles	Coating Remaining (%)
Al_2O_3	500	48.5 +/- 28.0
Al_2O_3	1000	73.0 +/- 22.3
Al_2O_3	1000 (following 7 days of aging)	95.1 +/- 6.9
TiO_2	500	70.1 +/- 26.5
TiO_2	1000	89.0 +/- 8.4

Observations indicate a reduction in coating loss with increased coating thickness for both the Al_2O_3 ALD or TiO_2 ALD coated samples. A shorter aging time of 7 days resulted in a much greater percentage of the coating remaining on the sample surface, supporting the model assumption that the bare areas expand as the aging time is increased.

The AFM results (Figure 5) indicate that a degree of island coalescence occurs in both of these coatings; however the finite radius of the probe does not allow fissures smaller than ≈ 10 nm to be detected, and the presence of such fissures could be the root cause behind this coating loss [31]. In principle the loss could also be due to thermal fracture [37]. Further experiments are

required to distinguish between these and other possibilities to constrain the root cause of coating delamination.

Defects in the ALD Coatings

Defects in ALD coatings have been widely discussed previously in the literature [28, 38, 39, 40] and are important to consider in the context of these experiments. As these coatings are intended to serve as diffusion barriers, slowing the transport of water to the glass surface, the presence of pinholes or fissures through the ALD films would impact the effectiveness of the applied coatings. Fick's first law for diffusion (Equation 1) can be utilized to describe the movement of water through the ALD barrier to the glass surface and to approximate the effect of the presence of such defects [41].

$$J = -D\frac{dC}{dx} \qquad \text{Equation 1}$$

where J is the flux, D is the diffusion coefficient of water or the H-bearing molecular species through the coating, C is its local concentration, and x is the depth beneath the sample surface. This one-dimensional form assumes the ALD coating is uniform and thus defect-free over the entire glass surface. While a defect-free coating is theoretically achievable, [26] in practice, defects are present depending on the condition of the surface to be coated and the growth mode [30]. Extended defects through the amorphous coating can play a similar role to that of grain boundaries or dislocations in a polycrystalline coating; they can provide a more rapid diffusive path for water or other H-bearing molecular species through the coating to the surface underneath. Such an accelerated path results in a change in the apparent *(app)* diffusivity of water or other hydrogen containing species through the coating D_{app} and which can be approximated by using Equation 2:

$$D_{apparent} = D_{coating} + D_{defect}(\frac{a}{A}) \qquad \text{Equation 2}$$

where $\left(\frac{a}{A}\right)$ is equal to the relative area fraction of defects and the *D* are the diffusion coefficients for the listed regions. The larger the defect area fraction present in the ALD coating, the greater the contribution of the higher diffusivity (D_{defect}) on the overall apparent diffusion coefficient. Thus, the efficacy of the applied ALD coatings can be directly impacted by the presence of defects in the coating [41].

Defects in ALD coatings can stem from at least two principal sources: incomplete coverage and thermal fracture. Incomplete coverage, either through growth suppression above unfavorable termination sites [39] or locally favorably-terminated sites on an otherwise unfavorably terminated substrate, [28, 29, 40] can result in pinholes or fissures through the applied ALD coating, respectively. These are illustrated in the schematics in Figure 9.

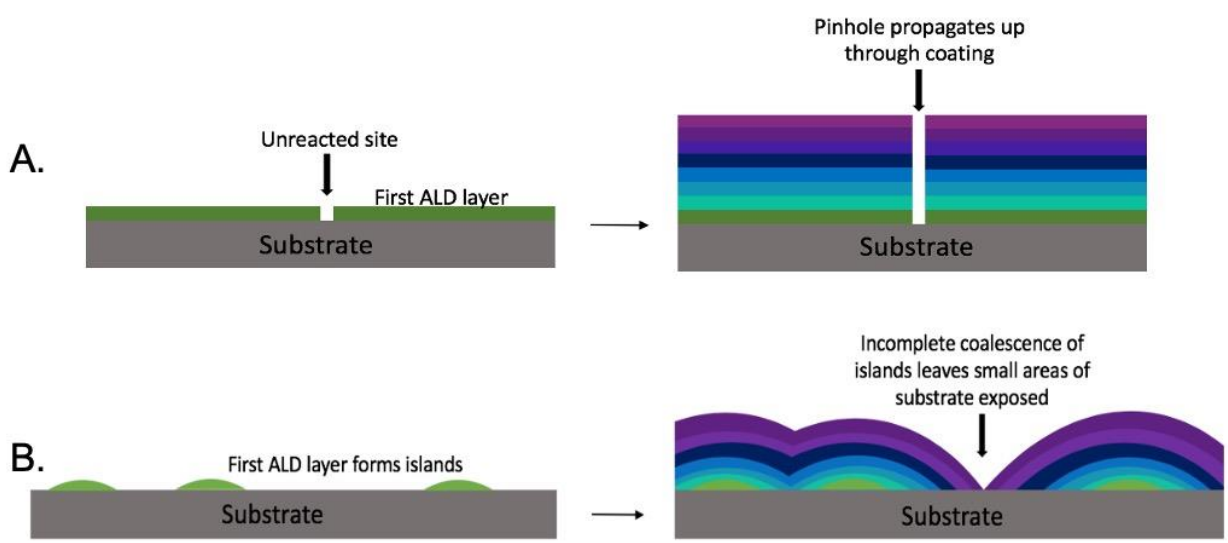

Figure 9: Schematic illustrations of pinhole formation by propagation (A) and non-linear deposition (island growth leading to fissure formation) (B).

Another important mode of defect formation in ALD coatings can be thermal fracture. ALD is typically performed at elevated temperatures (≈ 150°C) to allow for practical reaction and purge saturation times [27]. Differences in the coefficients of thermal expansion between the

ALD coating and the substrate results in stress as one of these (substrate or coating) contracts more than the other during sample cooling subsequent to deposition. The coefficients of thermal expansion are: 4.2 x 10^{-6} K^{-1} for Al_2O_3 ALD [42], 13.9 x 10^{-6} K^{-1} for TiO_2 ALD [43], and 8.0 x 10^{-6} K^{-1} for commercial float glass [44, 45]. These differences could result in the blistering (Al_2O_3) or fracturing (TiO_2) of the ALD coatings during cooling to room temperature, provided the thermal stress exceeds a critical value [37]. However, systematic experiments by Jen, et al. [46] showed that the critical compressive stress for crack formation for Al_2O_3 films on Teflon FEP substrates saturates with film thickness at a lower limiting value of approximately 1.8 GPa. This exceeds the thermal stress calculated for lowering the temperature from 150˚C to 25˚C, at 113 MPa, by more than an order of magnitude, and seemingly makes thermal fracture an unlikely source of failure of the ALD films studied here.

Conclusions:

The application of optically transparent Al_2O_3 films via atomic layer deposition was shown to dramatically decrease the release of select major elements (Si and Na) from float glass when immersed in water at elevated temperatures, and it is thus potentially a conservation treatment for glass in museum environments.

While the uptake of the elements by other solid phases formed during alteration cannot be excluded, and therefore artificial suppression of those elements in the altering solution, as another possible explanation for these results, such an explanation could be ruled out if the increasing concentration of Na and Si in the leachate scales with their depletion in the glass matrix. Experiments to test this are in progress.

In contrast, application of TiO_2 films did not significantly decrease the release of these elements. There are a number of possible reasons for the difference in performance between the two oxide coatings. It could be due to a difference in the rate, or saturation extent of coalescence of islands for the two types of oxides studied here, possibly because of the relative reactivity or sizes of the organometallic precursors used, respectively.

Our observations suggest that the limit to the efficacy of ALD Al_2O_3 coatings in mitigating glass alteration is set by delamination of the films when immersed in water; these may be nucleated at existing pinholes and/or fissure defects in applied ALD Al_2O_3 coatings on silicate glass. Further study is needed to test for the presence and role of such defects and what steps might prevent their formation.

<u>Abbreviations used in text:</u>

AFM: atomic force microscopy

ALD: atomic layer deposition

DI: deionized

EDS: energy dispersive spectrometry

ICP-MS: inductively coupled plasma mass spectrometry

PPM: parts per million (molar)

RMS: root-mean-square

SEM: secondary electron microscopy

TFE: tetrafluoroethylene

TDMAT: tetrakis(dimethylamido)titanium

TMA: trimethylaluminum

μXRF: micro-xray fluorescence

Declarations:

Disclaimer: Trade names and commercial products are identified in this paper to specify the experimental procedures in adequate detail. This identification does not imply recommendation or endorsement by the authors or by the National Institute of Standards and Technology, nor does it imply that the products identified are necessarily the best available for the purpose. Contributions of the National Institute of Standards and Technology and Museum Conservation Institute (a member of the Smithsonian Institution) are not subject to copyright.

Availability of data and materials: The datasets used and/or analyzed during the current study are available from the corresponding author on reasonable request.

Competing Interests: The authors declare that they have no competing interests.

Funding: Funding for this research came from several sources including a Smithsonian/University of Maryland Seed Grant awarded to RP and EPV and A Big Ten Academic Alliance Smithsonian Fellowship awarded to MEH, in addition to the A. James Clark School of Engineering at the University of Maryland.

Author's Contributions:

MH: prepared and ran experiments on the samples studied; performed the majority of the sample analysis; data reduction and analysis; prepared manuscript text.

JW: literature review support and guidance in experimental design, results interpretation and manuscript preparation.

TL: Assisted with sample analysis via SEM and color measurements.

NL: Assisted with and provided oversight and guidance for ICP-MS based sample analysis and data reduction.

EH: Assisted in sample preparation and analysis.

EV: Provided guidance and oversight in experimental design and development; oversaw and participated in SEM based analysis, optical imaging, data interpretation, and manuscript preparation.

RP: Oversaw experimental design development, data interpretation, and manuscript preparation.

All authors have reviewed and approved of the final version of this: 7/20/2020

Acknowledgements

The authors would like to acknowledge the contributions to this work made by undergraduate Saeed Bazroon, former Phaneuf Group member Dr. Amy Marquardt, John Abrams and the staff at the Nanofabrication Lab at the University of Maryland and the staff and imaging and analysis facilities at the Smithsonian Institution's Museum Conservation Institute.

References

[1] Strachan DM, Neeway J. Effects of alteration product precipitation on glass dissolution. Applied Geochemistry [Internet] 2014 June [cited 2020 Feb 10];45: 144-157. Available from: https://www.sciencedirect.com/science/article/abs/pii/S0883292714000675 DOI: 10.1016/j.apgeochem.2014.03.013

[2] Zanotto ED, Mauro JC. The glassy state of matter: Its definition and ultimate fate. Journal of Non-Crystalline Solids 471 (2017): 490-495. Available from: https://www.journals.elsevier.com/journal-of-non-crystalline-solids/highlighted-articles/the-glassy-state-of-matter-its-definition-and-ultimate-fate

[3] Gulbiten O, Mauro JC, Guo X, Boratav O. Viscous flow of medieval cathedral glass. Journal of American Ceramics Society [Internet] 2018 January [cited 2020 April 8] 101(1): 5-1. Available from: https://ceramics.onlinelibrary.wiley.com/doi/abs/10.1111/jace.15092

[4] Frankel GS, Vienna JD, Lian J, Scully JR, Gin S, Ryan JV, Wang J, Kim SH, Windl W, Du J. A comparative review of the aqueous corrosion of glasses, crystalline ceramics, and metals. NPJ

Materials Degradation [Internet]. 2018 April [cited 2020 Feb 10]; 2(15):1-17. Available from: https://www.nature.com/articles/s41529-018-0037-2
DOI: 10.1038/s41529-018-0037-2

[5] Brill RH. Crizzling – a problem in glass conservation. Studies in Conservation [Internet]. 1975 Jul [cited 2020 Feb 10]; 20(1):121-134. Available from: https://www.tandfonline.com/doi/abs/10.1179/sic.1975.s1.021
DOI: 10.1179/sic.1975.s1.021

[6] Vienna J, Kim DS, Skorski D, Matyas J. Glass property models and constraints for estimating the glass to be produced at Hanford by implementing current advanced glass formulation Efforts. PNNL-22631[Internet] 2013 Jul [cited 2020 Feb 10];1. Available from: https://www.osti.gov/biblio/1170502-glass-property-models-constraints-estimating-glass-produced-hanford-implementing-current-advanced-glass-formulation-efforts
DOI: 10.2172/1170502

[7] Jantzen CM, Brown KG, Pickett JB. Durable glass for thousands of years. International Journal of Applied Glass Science [Internet] 2010 March [cited 2020 Feb 10]; 1:38-62. Available from: https://ceramics.onlinelibrary.wiley.com/doi/abs/10.1111/j.2041-1294.2010.00007.x
DOI: 10.1111/j.2041-1294.2010.00007

[8] Naumann V, Lausch D, Hähnel A, Bauer J, Breitenstein O, Graff A, Werner M, Swatek S, Großer S, Bagdahn J, Hagendorf, C. Explanation of potential-induced degradation of the shunting type by Na decoration of stacking faults in Si solar cells. *Solar Energy Materials and Solar Cells [Internet] 2014 January [cited 2020 March 27]; 120(A)*:383-389. Available from: https://www.sciencedirect.com/science/article/pii/S0927024813003000

[9] Doremus RH. Interdiffusion of hydrogen and alkali ions in a glass surface. Journal of Non Crystalline Solids [Internet]. 1975 Dec [cited 2020 Feb 10];19:137-144. Available from: https://www.sciencedirect.com/science/article/abs/pii/0022309375900794
DOI:10.1016/0022-3093(75)90079-4

[10] Backhouse DJ, Fisher AJ, Neeway, JJ, et al. Corrosion of the International Simple Glass under acidic to hyperalkaline conditions. Mater Degrad [Internet]. 2018 Aug [cited 2020 Feb 10]; 2(29). Available from: https://www.nature.com/articles/s41529-018-0050-5
DOI:10.1038/s41529-018-0050-5

[11] Donatti, Dario A., Alberto Ibañez Ruiz, and Dimas R. Vollet. "A kinetic study of drying of TEOS-derived gels under nearly isothermal conditions." Materials Research 2.1 (1999): 43-47

[12] Frugier P, et al. SON68 nuclear glass dissolution kinetics: current state of knowledge and basis of the new GRAAL model. Journal of Nuclear Materials [Internet]. 2008 Oct [cited 2020 Feb 10];380(1-3):8-21. Available from: https://www.sciencedirect.com/science/article/pii/S0022311508003668
DOI: 10.1016/j.jnucmat.2008.06.044

[13] Hellmann, R, Cotte S, Cadel E, Malladi S, Karlsson LS, Lozano-Perez S, Cabié M, Seyeux A. Nanometre-scale evidence for interfacial dissolution–reprecipitation control of silicate glass corrosion. Nature Materials [Internet]. 2015 Jan [cited 2020 Feb 10]; 14:307-311. Available from: https://www.nature.com/articles/nmat4172#citeas
DOI: 10.1038/nmat4172

[14] Dal Bianco B. Investigation on sol-gel silica coatings for the protection of ancient glass: interaction with glass surface and protection efficiency. Journal of Non-Crystalline Solids [Internet] 2008 [cited 2020 Feb 10]; 354(26):2983-2992. Available from: https://www.researchgate.net/publication/239627095_Investigation_on_sol-gel_silica_coatings_for_the_protection_of_ancient_glass_Interaction_with_glass_surface_and_protection_efficiency
DOI: 0.1016/j.jnoncrysol.2007.12.004

[15] Wang B, Cunning B, Park S, Huang M, Kim J, Ruoff R. Graphene coatings as barrier layers to prevent the water-induced corrosion of silicate glass. American Chemical Society Nano [Internet] 2016 Oct [cited 2020 Feb 10]; 10(11):9794-9800. Available from: https://pubs.acs.org/doi/10.1021/acsnano.6b04363
DOI: 10.1021/acsnano.6b04363

[16] Maekawa S. editor. Oxygen Free Museum Cases. Getty Conservation Institute, Los Angeles. c1998.

[17] Rueden C, Dietz C, Horn M, Schindelin J, Northan B, Berthold M, Eliceiri K. (2016). ImageJ Ops [Software]. https://imagej.net/Ops.

[18] Friel, J. J., R. Terborg, S. Langner, T. Salge, M. Rohde, and J. Berlin. X-Ray and Image Analysis in Electron Microscopy.. Pro Buisness Verlag 3rd ed. c2017.

[19] Vicenzi EP, Eggins S, Logan AL, and Wysoczanski W Microbeam Characterization of Corning Archeological Reference Glasses: New Additions to the Smithsonian Microbeam Standard Collection. Journal Research Natl. Inst. Standards Technol. 2002 Dec. [cited 2020 Feb 10];107:719–727. Alible from: https://www.ncbi.nlm.nih.gov/pmc/articles/PMC4863856/

DOI:10.6028/jres.107.058

[20] Gateau P. Solubility of tin oxide in soda-lime silicate melts. Journal of Non-crystalline Solids [Internet]. 2012 April [cited 2020 Feb 10];358(8):135-1140. Available from: https://www.sciencedirect.com/science/article/abs/pii/S002230931200083X
DOI: 10.1016/j.jnoncrysol.2012.02.009

[21] Code of Ethics. American Institute of Conservation. 2019. https://www.culturalheritage.org/about-conservation/code-of-ethics. Accessed 2020 April 8.

[22] Marquardt AE. Novel protective coatings for silver and copper alloy cultural heritage objects using atomic layer deposited metal oxide barrier films. Doctoral Dissertation, University

of Maryland College Park. December 2015 [cited 2020 April 24]. Available from: https://drum.lib.umd.edu/handle/1903/17239

[23] Abdulagatov A, Yan Y, Cooper J, Zhang Y, Gibbs Z, Cavanagh A, Yang R, Lee Y, George S Al2O3 and TiO3 atomic layer deposition on copper for water corrosion resistance, American Chemical Society Applied Material Interfaces [Internet]. 2011 Dec [cited 2020 Feb 10];3(12):4593-601. Available from: https://www.ncbi.nlm.nih.gov/pubmed/22032254 DOI: 10.1021/am2009579

[24] Haschke M, Boehm S. Advances in Imaging and Electron Physics, Chapter 1: Micro-XRF in Scanning Electron Microscopes, Vol 199, pg 1-60. Elsevier Inc. c2017. ISN: 1076-5670

[25] ASTM C1285 – 14. Standard Test Methods for Determining Chemical Durability of Nuclear, Hazardous, and Mixed Waste Glasses and Multiphase Glass Ceramics: The Product Consistency Test (PCT). ASTM International. Accessed 2020 Jan 10.

[26] Puurunen RL. Surface chemistry of atomic layer deposition: A case study for the trimethylaluminum/water process. Journal of applied physics [Internet] 2005 April [cited 2020 Feb 10]; 97(121301). Available from: https://aip.scitation.org/doi/10.1063/1.1940727

[27] George SM. Atomic layer deposition: an overview. Chem Rev [Internet]. 2009 Feb [cited 2020 Feb 10]; 110(1):111-131. Available from: https://pubs.acs.org/doi/10.1021/cr900056b DOI: 10.1021/cr900056b

[28] Puurunen RL, Vandervorst W, Besling W, Richard O, Bender H, Conard T, Zhao C et al. Island growth in the atomic layer deposition of zirconium oxide and aluminum oxide on hydrogen-terminated silicon: Growth mode modeling and transmission electron microscopy. Journal of applied physics [Internet] 2004 Oct [cited 2020 Feb 10];96(9): 4878-4889. Available from: https://aip.scitation.org/doi/abs/10.1063/1.1787624?journalCode=jap DOI: 10.1063/1.1787624

[29] McDonnell S, et al. Controlling the atomic layer deposition of titanium dioxide on silicon: dependence on surface termination. The J of Phys Chem C [Internet] 2013 Sept [cited 2020 Feb 10]; 117(39): 20250-20259. Available from https://pubs.acs.org/doi/abs/10.1021/jp4060022 DOI: 10.1021/jp4060022

[30] Yerzak A, Lee Y. Probabilistic distributions of pinhole defects in atomic layer deposited films on polymeric substrates. Journal of Vacuum Science and Technology A: Vacuum, Surfaces and Films [Internet] 2016 Jan [cited 2020 Feb 10]; 34(1). Available from: h

[31] Westra KL, Thomson DJ. Effect of tip shape on surface roughness measurements from atomic force microscopy images of thin films. Journal of Vacuum Science and Technology B: Microelectronics and Nanometer Structures Processing Measurement and Phenomena. 1995 December [cited 2020 April 14]; 13(2) 344-349. Available from: http://doi.org/10.1116/1.587943

[32] Feldmann M, Weiβmann R. Initial stages of float glass corrosion. Journal of Non-Crystalline Solids [Internet] 1997 Sept. [cited 2020 July 1]; 218: 205-209. Available from: https://doi.org/10.1016/S0022-3093(97)00277-9

[33] Jantzen CM, Trivelpiece CL, Crawford CL, Pareizs JM, Pickett, JB. Accelerated Leach Testing of Glass (ALTGLASS): II. Mineralization of hydrogels by leachate strong bases. International Journal of Applied Glass Science [Internet] 2017 Feb [cited 2020 March 23];8(1): 84-96. Available from: https://ceramics.onlinelibrary.wiley.com/doi/abs/10.1111/ijag.12264

[34] Sung CJ, Kim H-J, Choi JW, Han YK. Sodium diffusion in Al_2O_3: a distinct perspective compared with lithium ion diffusion. Nano Letters, Oct 2014 [cited 2020 April 30]; 14: 6559-6563. DOI: 10.1021/nl503169v

[35] Moller J, Reiche D, Bobeth M, Pompe W. Observations of boron nitride thin film delamination due to humidity. Surface and Coatings Technology. [Internet] 2002 Feb. [cited 2020 July 1]; 150: 8-14
DOI: 10.1016/S0257-8972(01)01500-6

[36] Cardinale GF, Mirkarimi PB, McCarty KF, Klaus EJ, Medlin DL, Clift WM. Effects of ambient conditions on the adhesion of cubic boron nitride films on silicon substrates. Thin Solid Films [Internet] 1994 Dec. [cited 2020 July 1]; 253(1-2): 130-135. Available from: https://doi.org/10.1016/0040-6090(94)90307-7

[37] Hutchinson JW. Stresses and failure modes in thin films and multilayers. Notes for a DCAMM Course: Technical University of Denmark, Lyngby. October 1996 [cited 2020 Feb 10] Available from: https://www.seas.harvard.edu/hutchinson/papers/462-5.pdf

[38] Carcia PF, Mclean RS, Reilly MH. Ca test of Al2O3 gas diffusion barriers grown by atomic layer deposition on polymers. Applied Physics Letters [Internet]. 2006 May [cited 2020 Feb 10]; 89(031915). Available from:
https://aip.scitation.org/doi/abs/10.1063/1.2221912?journalCode=apl
DOI: 10.1063/1.2221912

[39] Carcia PF, McLean RS, Groner MD, Dameron AA, George SM. Gas diffusion ultrabarriers on polymer substrates using Al2O3 atomic layer deposition and SiN plasma-enhanced chemical vapor deposition. Journal of Applied Physics [Internet]. 2009 [cited 2020 Feb 10];106(023533) Available from: https://aip.scitation.org/doi/abs/10.1063/1.3159639?journalCode=jap
DOI: 10.1063/1.3159639

[40] Puurunen RL, Vandervorst W. Island growth as a growth mode in atomic layer deposition: A phenomenological model. Journal of Applied Physics [Internet] 2004 Sept [cited 2020 Feb 10]; 96(12): 7686-7695. Available from: https://aip.scitation.org/doi/10.1063/1.1810193
DOI: 10.1063/1.1810193

[41] Porter, D. A., Easterling, K. E. & Sherif, M. Y. Phase Transformations in Metals and Alloys, 3rd ed. Van Nostrnad Reinhold Co. Ltd, UK, c2009.

[42] Miller D, Foster R, Jen S, Bertrand J, Cunningham S, Morris A, Lee Y, George S, Dunn A. Thermo-mechanical properties of alumina films created using the atomic layer deposition technique. Sensors and Actuators A: Physical [Internet] 2010 Nov [cited 2020 Feb 10];164(1-2):58-67 Available from: https://www.sciencedirect.com/science/article/abs/pii/S0924424710004292 DOI: 10.1016/j.sna.2010.09.018

[43] Saleem M, Honkanen S, Turunen J. Thermal properties of TiO_2 films fabricated by atomic layer deposition, International Symposium on Advanced Materials [Internet] 2013 [cited 2020 Feb 10];60(1). Available from: https://iopscience.iop.org/article/10.1088/1757-899X/60/1/012008/meta

[44] Barrett, C, Nix W, Tetelman A. The Principles of Engineering Materials, Englewood Cliffs: Prentice-Hall Inc.; c1973.

[45] Hidnert P. Thermal expansion of five selected optical glasses. Journal of Research of the National Bureau of Standards [Internet] 1954 June [cited 2020 Feb 10]; 52(6):311-312 . Available from: https://nvlpubs.nist.gov/nistpubs/jres/52/jresv52n6p311_a1b.pdf

[46] Jen S, Bertrand J, George S. Critical tensile and compressive strains for cracking of Al_2O_3 films grown by atomic layer deposition. Journal of Applied Physics [Internet] 2011 April [cited 2020 January 10];109:084305. Available from: https://aip.scitation.org/doi/abs/10.1063/1.3567912 DOI: 10.1063/1.3567912